Magneto-optical trapping and sub-Doppler cooling of a polyatomic molecule

https://doi.org/10.1038/s41586-022-04620-5

Received: 17 December 2021

Accepted: 4 March 2022

Published online: 1 June 2022

Check for updates

Nathaniel B. Vilas[1,2]✉, Christian Hallas[1,2], Loïc Anderegg[1,2], Paige Robichaud[1,2], Andrew Winnicki[1,2], Debayan Mitra[1,2,3] & John M. Doyle[1,2]

Laser cooling and trapping[1,2], and magneto-optical trapping methods in particular[2], have enabled groundbreaking advances in science, including Bose–Einstein condensation[3–5], quantum computation with neutral atoms[6,7] and high-precision optical clocks[8]. Recently, magneto-optical traps (MOTs) of diatomic molecules have been demonstrated[9–12], providing access to research in quantum simulation[13] and searches for physics beyond the standard model[14]. Compared with diatomic molecules, polyatomic molecules have distinct rotational and vibrational degrees of freedom that promise a variety of transformational possibilities. For example, ultracold polyatomic molecules would be uniquely suited to applications in quantum computation and simulation[15–17], ultracold collisions[18], quantum chemistry[19] and beyond-the-standard-model searches[20,21]. However, the complexity of these molecules has so far precluded the realization of MOTs for polyatomic species. Here we demonstrate magneto-optical trapping of a polyatomic molecule, calcium monohydroxide (CaOH). After trapping, the molecules are laser cooled in a blue-detuned optical molasses to a temperature of 110 μK, which is below the Doppler cooling limit. The temperatures and densities achieved here make CaOH a viable candidate for a wide variety of quantum science applications, including quantum simulation and computation using optical tweezer arrays[15,17,22,23]. This work also suggests that laser cooling and magneto-optical trapping of many other polyatomic species[24–27] will be both feasible and practical.

Polyatomic molecules, including calcium monohydroxide (CaOH), have distinct degrees of freedom that make them powerful tools for quantum science. For example, the rotation of polyatomic molecules about their internuclear axis generically results in nearby levels of opposite parity, leading to fully polarized quantum states with linear Stark shifts at low electric field, as well as states with zero first-order electric field sensitivity[15]. Such states are predicted to be useful for research in quantum simulation and computation, ultracold collisions and beyond-the-standard-model searches[15–18,20]. For CaOH, this parity doublet structure is obtained in the low-lying vibrational bending modes[18,20]. Motivated by the diverse applications of polyatomic molecules at the frontier of quantum physics and chemistry, several techniques have previously demonstrated trapping and/or cooling of polyatomic molecules. Methyl (CH_3) radicals have been trapped in a permanent magnetic trap[28], and trapped formaldehyde (H_2CO) molecules have been cooled below 1 mK by electro-optic Sisyphus cooling[29,30]. Although polyatomic molecules including strontium monohydroxide (SrOH)[31], CaOH[32], ytterbium monohydroxide (YbOH)[33] and calcium monomethoxide ($CaOCH_3$)[34] have all been laser cooled in one dimension, polyatomic molecules have not previously been trapped and cooled in a magneto-optical trap (MOT). A MOT relies on dissipative scattering of thousands of photons from lasers that are tuned into or out of resonance according to the molecules' positions and velocities in a quadrupole magnetic field[2]. This leads to simultaneous trapping and cooling to near the Doppler limit, in the millikelvin temperature regime or below. The rapid cooling and compression provided by MOTs is highly desirable for efficiently increasing the phase-space density of the trapped species, and because of this, MOTs are the workhorse tool in ultracold atomic physics.

In this work, we extend magneto-optical trapping to a polyatomic molecule, CaOH. This is accomplished by optical photon cycling of CaOH sufficient to enable laser slowing, trapping in a MOT and cooling to temperatures near the Doppler limit. To cool to even lower temperatures, we apply a blue-detuned optical molasses, reaching temperatures below the Doppler limit. In addition to trapping and cooling, this work demonstrates the photon cycling needed to perform high-fidelity quantum-state readout in polyatomic molecules. The realized density and temperature represent a viable starting point for further laser cooling to lower temperatures[35–38] and the loading of CaOH molecules into optical dipole trap arrays[22,37,39]. Application to a wide variety of molecules analogous to CaOH where, for example, the OH group is replaced by a complex ligand, has been proposed[25,26]. This work also suggests that MOTs of such molecules, for example, CaSH and $CaOCH_3$, are within reach[25,26].

CaOH laser cooling and MOT loading

Our experiment begins with a cryogenic buffer gas beam[40] of CaOH molecules produced in a two-stage buffer gas cell cooled to about 2 K.

[1]Department of Physics, Harvard University, Cambridge, MA, USA. [2]Harvard-MIT Center for Ultracold Atoms, Cambridge, MA, USA. [3]Present address: Department of Physics, Columbia University, New York, NY, USA. ✉e-mail: vilas@g.harvard.edu

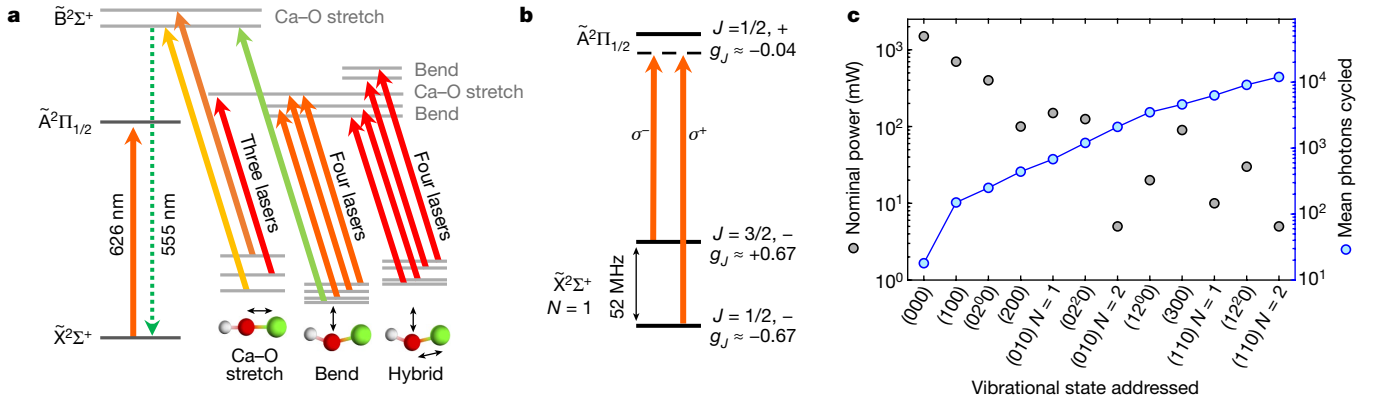

Fig. 1 | Laser cooling and repumping scheme. a, The primary cycling transition for slowing and the MOT is the $\tilde{X}^2\Sigma^+ \leftrightarrow \tilde{A}^2\Pi_{1/2}$ transition at 626 nm. Spontaneous decay from the laser repumping the first Ca–O stretching mode is at 555 nm and is used for background-free imaging. Decays to Ca–O stretch, bend and hybrid vibrational modes in the electronic ground state are repumped though a number of excited vibronic states to attain a closure of approximately 12,000 photons (Methods). **b**, CaOH MOT polarization configuration. The MOT beams addressing the $\tilde{X}(N''=1, J''=3/2, p''=-)$ and $\tilde{X}(N''=1, J''=1/2, p''=-)$ ground states have opposite polarization due to their opposite g-factors (or magnetic moments), g_J. **c**, The power of each slowing and repumping laser required to saturate the laser slowing and MOT efficacy (left axis; black). The right axis (blue) shows the mean number of photons, before 1/e loss of molecular population occurs, by adding all preceding repumping lasers (from left to right)[47,48]. Lasers are labelled by the vibrational state repumped, notated as $(v_1 v_2^{\ell} v_3)$, where v_1, v_2 and v_3 are the vibrational quantum numbers for the Ca–O stretch, Ca–O–H bend and O–H stretch modes, respectively, and ℓ is the projection of the vibrational angular momentum onto the molecular axis.

In brief, a metal calcium target in the cell is ablated, producing calcium atoms that react in the gas phase with water (H_2O), which is introduced through a heated capillary into the cell. CaOH production via a Ca–H_2O reaction is enhanced by optically exciting the reactant calcium atoms to the metastable $4s4p^3P_1$ state (Methods)[41]. CaOH molecules exit the cell with a peak forward velocity of $v_f \approx 140$ m s^{-1} and a flux of about 5×10^{10} molecules per steradian per pulse in the $N''=1$ rotational state used for laser cooling (where N' is the rotational quantum number in the electronic ground state).

As the CaOH molecules travel from the cell to the MOT region, which is 81 cm downstream, they are illuminated with counter-propagating white-light slowing lasers[42–46], including the 'main' 626-nm $\tilde{A}^2\Pi_{1/2}(J'=1/2, p'=+) \leftarrow \tilde{X}^2\Sigma^+(N''=1, p''=-)$ cycling transition (Methods)[32]. Here J' and p' are the total angular momentum and parity of the excited state, respectively, and p'' is the parity of the ground state. Given the recoil velocity of $\hbar k/m \approx 1.1 \times 10^{-2}$ m s^{-1} (where $\hbar$ is the reduced Planck constant, $k = 2\pi/(626\text{ nm})$ and $m = 57$ atomic mass units is the mass of CaOH), approximately 10,000 photons must be scattered per molecule to slow the velocity peak of the molecular beam to below the MOT capture velocity ($\lesssim$10 m s^{-1})[32]. Additional 'repumping' lasers copropagate with the main cycling light and repump population that decays to three Ca–O stretching vibrational modes, three Ca–O–H bending modes and three mixed character modes (Fig. 1a)[47,48]. Two more lasers are added for rotational repumping of vibrational modes with a parity doublet structure[47]. The suite of repumpers allows for approximately 12,000 photons to be scattered before 1/e ≈ 36.8% of the initial molecular population remains, while the rest is lost to unaddressed vibrational states (Methods)[48]. As we will describe, this number is amply sufficient for laser slowing and subsequent cooling and trapping in a MOT.

The main cycling and repumping lasers used for slowing are frequency-broadened by about 300 MHz so that molecules with velocities as high as 140 m s^{-1} can be slowed to rest in the MOT region. The counter-propagating slowing light interacts with the CaOH molecular beam along the full slowing length and is focused from a 1/e^2 Gaussian diameter of 11.5 mm at the MOT region to a 5.5-mm diameter at the buffer gas cell. The focusing provides transverse compression forces and has been shown to improve slowing efficiency in experiments with diatomic molecules[46,49]. The polarization of each slowing laser is rapidly switched at about 1.4 MHz between two orthogonal linear polarizations using a Pockels cell, ensuring remixing of magnetic dark states in the cycling scheme over the full slowing length[50]. The minimum laser powers required to saturate the slowing effect on the molecules, as well as to optimize the trapping and cooling efficacy, are plotted in Fig. 1c (Methods). Notably, over half of the frequency-broadened repumping lasers require less than 100 mW, a technically straightforward requirement. These powers could be further reduced by using slowing techniques that do not rely on spectrally broadened lasers.

The optical cycle for trapping CaOH is formed by addressing the $\tilde{X}^2\Sigma^+(N''=1, J''=1/2, p''=-)$ and $\tilde{X}^2\Sigma^+(N''=1, J''=3/2, p''=-)$ components (where J'' is the total angular momentum) of the electronic ground state, 52 MHz apart (Fig. 1b). Both components are driven to the $\tilde{A}^2\Pi_{1/2}(J'=1/2, p'=+)$ excited electronic level, and their polarizations are chosen to preferentially scatter photons from the confining MOT laser beams (Fig. 1b)[51]. Magnetic dark states that occur in these 'type II' transitions are remixed by rapidly switching laser polarizations between σ^+ and σ^- with a Pockels cell at 1.0 MHz. Trapping is maintained by modulating the current through the anti-Helmholtz MOT coils in phase with the polarization switching[11,12,32,52,53]. Each of the six MOT beams has a 1/e^2 Gaussian diameter of 10 mm (truncated at a diameter of 19 mm by in-vacuum baffles), and the laser power in each beam is equally balanced between the $\tilde{X}(N''=1, J''=3/2, p''=-)$ and $\tilde{X}(N''=1, J''=1/2, p''=-)$ components. The axial radio-frequency magnetic field gradient has a root-mean-square value of about 8.5 G cm^{-1}.

The experimental sequence used to load the MOT is as follows. The slowing lasers are turned on 1 ms after ablation of the calcium target, and are held at constant power for a duration of 23 ms. During this time, the MOT beams are held at a power of 33 mW per beam with a detuning of -2.0Γ, where $\Gamma = 2\pi \times 6.4$ MHz is the natural linewidth of the cooling transition. When the slowing beam is turned off, the intensity in each MOT laser beam is ramped down to 3 mW over 5 ms, and the detuning is simultaneously ramped to -0.9Γ. All repumping lasers that are used for slowing (that is, all except for the main cycling laser at 626 nm) are kept on for the full MOT sequence to address vibrational and rotational dark states inside the MOT. Thus, the same frequency-broadened repumping lasers are used for repumping molecules during all three tasks of the experiment: slowing, magneto-optical trapping and sub-Doppler cooling (see below).

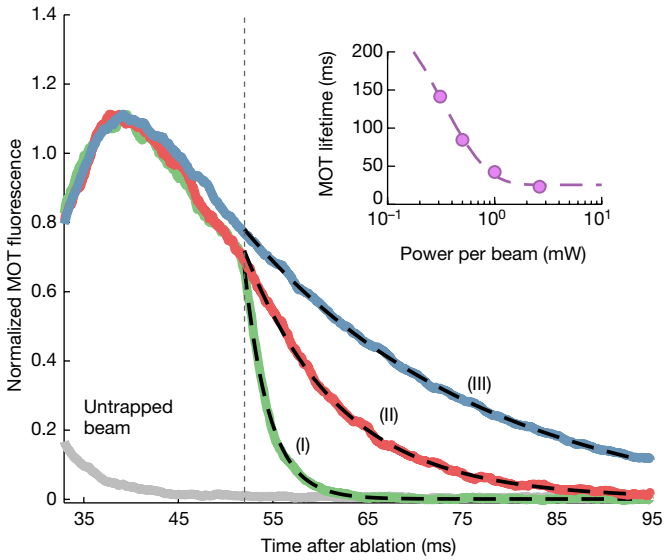

Fig. 2 | MOT lifetime versus number of states repumped. CaOH fluorescence is plotted as a function of time for an untrapped molecular beam (grey curve), and for molecules trapped in the MOT, with select repumpers switched off at 52 ms (vertical dashed line; curves I–III). The configurations achieve 1/e population loss after 1,200 photons scattered (5 repumping lasers; I), 4,600 photons (8 repumpers; II) and ~12,000 photons (11 repumpers; III). I–III are normalized to their mean signal from 35 ms to 52 ms. The untrapped beam is normalized to the average of I–III from 1 ms to 35 ms (during which time fast, untrapped molecules pass through the MOT region). The dotted lines are exponential fits, from which we extract MOT lifetimes of 2.60(3) ms, 10.1(2) ms and 25.7(6) ms for I–III, respectively. Errors are 1σ fit errors. Inset: MOT lifetime versus power per MOT beam. The dotted line is a guide to the eye..

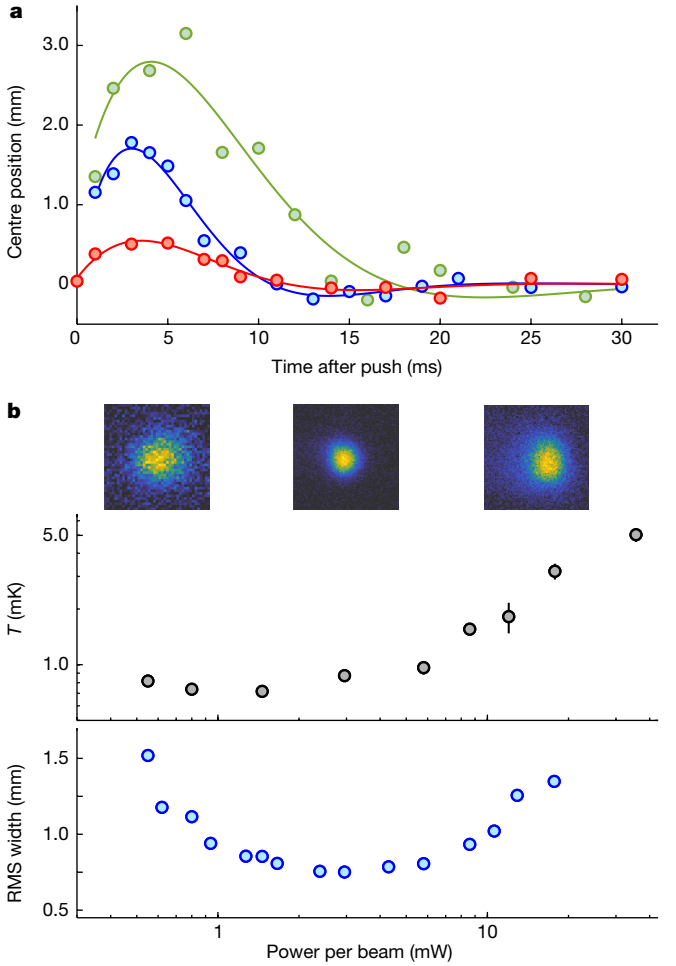

Fig. 3 | MOT dynamics and characteristics. a, CaOH cloud position as a function of time after a sudden displacement, for MOT powers of 1.2 mW (green; top curve), 3 mW (blue; middle curve) and 11.5 mW (red; bottom curve). The fitted MOT parameters are $\beta = \{310(90), 455(85), 340(100)\}$ s^{-1} and $\omega = 2\pi \times \{37(4), 59(4), 50(4)\}$ Hz for the three powers, respectively. **b**, Geometric mean temperature, $T = T_{\mathrm{radial}}^{2/3} T_{\mathrm{axial}}^{1/3}$ (middle plot; black) and geometric root mean square (RMS) width (bottom plot; blue) of the CaOH MOT versus laser power in each MOT beam. Error bars are 1σ fit errors and are smaller than the plot markers for most points. CaOH MOT images are shown at top for representative powers of 0.5 mW, 3.0 mW and 12.9 mW per MOT beam, from left to right. The MOT is imaged for 10 ms following a 15-ms wait time to fully thermalize. The image size is 7 × 7 mm. The three intensity axes are different owing to changing numbers and scattering rates at each MOT power. Normalized to the centre image, the maximum image intensity from left to right is 0.23, 1 and 0.38.

Characterization of the MOT

To characterize the MOT, we collect fluorescence photons emitted at 555 nm resulting from spontaneous emission on the $\tilde{B}^2\Sigma^+ \rightarrow \tilde{X}^2\Sigma^+$ transition. In our photon cycling scheme, approximately 1 out of every 18 photons scattered during laser cooling occurs at this wavelength (Fig. 1a, Methods). This imaging scheme enables background-free detection owing to the absence of cooling or repumping lasers at 555 nm. As shown in Fig. 2, the MOT manifests itself as a persistence of molecular fluorescence (collected on a photomultiplier tube) at long times after the slowed molecular beam has fully passed through the trapping region. The signal is observed to decay exponentially owing to molecules being lost from optical cycling into higher vibrational dark states. By selectively removing repumping lasers during trapping, the average number of photon scatters during cooling may be varied. We observe that the MOT lifetime depends linearly on the number of photons scattered, as expected. We extract from the lifetime measurements a scattering rate of $4.6(1) \times 10^5$ s^{-1} (Methods). By decreasing the intensity of the MOT laser beams after initial loading, the overall scattering rate can be reduced, extending the MOT lifetime beyond 100 ms (Fig. 2, inset).

Next, we measure the cooling of molecules and the damping of their motion in the MOT. The MOT forces may be approximated at low velocity and displacement as those of a damped harmonic oscillator, $F/m = -\beta v - \omega^2 r$. Here v and r are the velocity and position in the trap, and β and ω are the damping constant and trap frequency, respectively. To measure these properties, we observe the MOT after an intentional spatial displacement (Methods). After loading the MOT and ramping the MOT light to a power of 3 mW per beam, the slowing laser is turned on for 1 ms to displace the cloud of CaOH molecules from its equilibrium position. After a variable wait time, the molecules are imaged for 1 ms on an electron-multiplying charge-coupled device (EMCCD) camera and the centre position is extracted (Fig. 3a). We measure a damping constant $\beta = 455(85)$ s^{-1} and an oscillation frequency $\omega = 2\pi \times 59(4)$ Hz. The observed damping constant and frequency are comparable to those achieved in MOTs of diatomic molecules[10,11]. Moreover, the characteristic damping time $\beta^{-1} \approx 2.2$ ms at this intensity is much shorter than the 1/e MOT lifetime of 25.7(6) ms (Fig. 2), indicating that significant cooling and compression of the MOT is possible. The damping is lower for MOT laser powers both above and below the optimum (Fig. 3a), as expected[54].

The temperature of the molecules in the MOT is measured by time-of-flight (TOF) expansion. The MOT light is held at fixed power for about 15 ms following the initial ramp, and then the MOT lasers and anti-Helmholtz coils are simultaneously turned off. After a variable time τ_{TOF}, an image of the expanded molecular cloud is taken. The expanded cloud widths, σ, are determined from two-dimensional (2D) Gaussian fits, and the radial and axial MOT temperatures are extracted

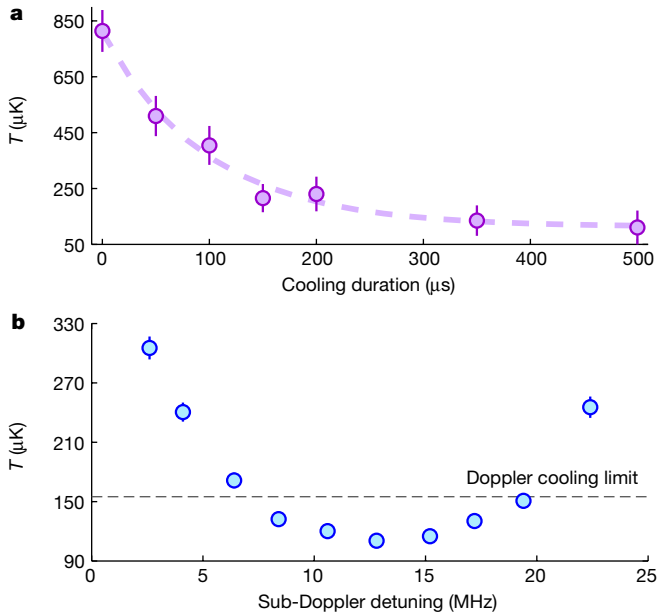

Fig. 4 | Sub-Doppler cooling. a, Temperature as a function of cooling duration. The dotted line is an exponential fit, from which we extract a 1/e cooling time of 98(15) μs. **b**, Temperature as a function of sub-Doppler detuning Δ_{SD}. The Doppler cooling limit for CaOH is shown as a dotted line. Error bars for both panels are 1σ fit errors derived from 2D Gaussian fits of the expanded molecular cloud widths.

from a linear fit of σ^2 versus τ_{TOF}^2 (Methods). The final MOT temperature depends strongly on the MOT power (Fig. 3b) owing to sub-Doppler heating effects[55], as have been observed in other type II MOTs[11,53]. As the power is lowered, the temperature of the MOT reaches a minimum measured temperature of 720(40) μK.

Following the 5-ms loading ramp and a roughly 15 ms hold at variable intensity, the diameter of the molecular cloud is determined by imaging the MOT with a 10-ms EMCCD exposure. The diameter is smallest at a power of 3 mW per MOT beam (Fig. 3c), increasing at both lower and higher intensities. After about 15 ms of cooling at 3 mW per MOT beam, we observe approximately 20,000 molecules (Methods) with a temperature of 870(50) μK, a peak number density of $3.0(1.5) \times 10^6$ cm^{-3}, and a peak phase-space density of $1.4(7) \times 10^{-12}$. These values are all comparable to those achieved in the first MOTs of diatomic molecules[9–12]. The MOT could be further improved by repumping additional, known, vibrational loss channels[48].

Sub-Doppler cooling of CaOH

We sub-Doppler cool the molecular cloud by applying a blue-detuned optical molasses. As demonstrated previously for diatomic molecules with the type II $J \rightarrow J-1$ transitions used here[10,39,56], the presence of dark states in the ground manifold leads to polarization gradient forces that result in strong sub-Doppler heating at red detuning and sub-Doppler cooling at blue detuning[55,57]. After loading and cooling the MOT, we perform sub-Doppler cooling by turning off the MOT coils, MOT lasers and the polarization switching over a period of 130 μs, and simultaneously jumping both frequency components of the MOT lasers to a variable detuning Δ_{SD}. The cooling laser beams are then switched on for 1 ms at a power of 30 mW per beam. After this cooling pulse, the CaOH temperature is measured via TOF expansion, as described above. The cooling occurs with a characteristic time of 98(15) μs (Fig. 4a) and a scattering rate of $7.7(4) \times 10^5$ s^{-1}, corresponding to only 75 photon scatters for a 1/e decrease in temperature. We find an optimal detuning of $\Delta_{SD} = +13$ MHz (Fig. 4b). As the lower-frequency component of the sub-Doppler cooling light is red-detuned from the $\tilde{A}(J'=1/2, p'=+) \leftarrow \tilde{X}(N''=1, J''=1/2, p''=-)$ transition, sub-Doppler heating might be possible as the detuning increases. The minimum temperature acheived is 110(4) μK, which is comparable to the temperatures achieved in diatomic molecules using a similar cooling mechanism[10,11,36].

Conclusion and outlook

We have demonstrated magneto-optical trapping of a polyatomic molecule, CaOH, and performed sub-Doppler cooling to reach temperatures below the Doppler laser cooling limit. We expect that lower temperatures may be achieved by using techniques that were used to sub-Doppler cool diatomic molecules to 10 μK (refs. [35–37]). At such temperatures, loading CaOH molecules into conservative optical traps, including optical tweezer arrays, will be possible[22,37,39,58]. Such a platform would enable the ability to study and engineer interactions between individual, ultracold CaOH molecules, using nearby opposite parity states in the vibrational bending mode[15–17,20,59]. We have demonstrated the ability to rapidly scatter >10^4 photons in CaOH, which will greatly aid in achieving the high-fidelity state preparation and detection required for these quantum simulation and computation applications[15–17,59], as well as beyond-the-standard-model searches[20,21]. Finally, this work is a proof of principle that managing rovibrational loss channels in polyatomic molecules for the purpose of laser cooling is feasible in species with optically accessible transitions and branching losses similar to those of CaOH. This is particularly notable as recent theoretical and experimental work indicates that these criteria are satisfied not only by linear, triatomic molecules but also by several classes of molecules of even greater structural complexity. Several candidate species have already been identified, spanning nonlinear symmetric top molecules (for example, $CaOCH_3$ and $SrOCH_3$)[25], asymmetric top molecules (for example, CaSH and $CaNH_2$)[26] and complex organic molecules containing carbon rings (for example, $CaOC_6H_5$ and $SrOC_9H_2F_9$)[27,60].

Online content

Any methods, additional references, Nature Research reporting summaries, source data, extended data, supplementary information, acknowledgements, peer review information; details of author contributions and competing interests; and statements of data and code availability are available at https://doi.org/10.1038/s41586-022-04620-5.

1. Phillips, W. D. Nobel lecture: Laser cooling and trapping of neutral atoms. *Rev. Mod. Phys.* **70**, 721–741 (1998).
2. Chu, S. Nobel lecture: The manipulation of neutral particles. *Rev. Mod. Phys.* **70**, 685–706 (1998).
3. Cornell, E. A. & Wieman, C. E. Nobel lecture: Bose–Einstein condensation in a dilute gas, the first 70 years and some recent experiments. *Rev. Mod. Phys.* **74**, 875–893 (2002).
4. Anderson, M. H., Ensher, J. R., Matthews, M. R., Wieman, C. E. & Cornell, E. A. Observation of Bose–Einstein condensation in a dilute atomic vapor. *Science* **269**, 198–201 (1995).
5. Davis, K. B. et al. Bose–Einstein condensation in a gas of sodium atoms. *Phys. Rev. Lett.* **75**, 3969–3973 (1995).
6. Bernien, H. et al. Probing many-body dynamics on a 51-atom quantum simulator. *Nature* **551**, 579–584 (2017).
7. Levine, H. et al. Parallel implementation of high-fidelity multiqubit gates with neutral atoms. *Phys. Rev. Lett.* **123**, 170503 (2019).
8. Ludlow, A. D., Boyd, M. M., Ye, J., Peik, E. & Schmidt, P. O. Optical atomic clocks. *Rev. Mod. Phys.* **87**, 637–701 (2015).
9. Barry, J. F., McCarron, D., Norrgard, E., Steinecker, M. & DeMille, D. Magneto-optical trapping of a diatomic molecule. *Nature* **512**, 286–289 (2014).
10. Truppe, S. et al. Molecules cooled below the Doppler limit. *Nat. Phys.* **13**, 1173–1176 (2017).
11. Anderegg, L. et al. Radio frequency magneto-optical trapping of CaF with high density. *Phys. Rev. Lett.* **119**, 103201 (2017).
12. Collopy, A. L. et al. 3D magneto-optical trap of yttrium monoxide. *Phys. Rev. Lett.* **121**, 213201 (2018).
13. Micheli, A., Brennen, G. & Zoller, P. A toolbox for lattice-spin models with polar molecules. *Nat. Phys.* **2**, 341–347 (2006).

14. Safronova, M. S. et al. Search for new physics with atoms and molecules. *Rev. Mod. Phys.* **90**, 025008 (2018).
15. Yu, P., Cheuk, L. W., Kozyryev, I. & Doyle, J. M. A scalable quantum computing platform using symmetric-top molecules. *New J. Phys.* **21**, 093049 (2019).
16. Wall, M. L., Maeda, K. & Carr, L. D. Simulating quantum magnets with symmetric top molecules. *Ann. Phys.* **525**, 845–865 (2013).
17. Wall, M., Maeda, K. & Carr, L. D. Realizing unconventional quantum magnetism with symmetric top molecules. *New J. Phys.* **17**, 025001 (2015).
18. Augustovičová, L. D. & Bohn, J. L. Ultracold collisions of polyatomic molecules: CaOH. *New J. Phys.* **21**, 103022 (2019).
19. Heazlewood, B. R. & Softley, T. P. Towards chemistry at absolute zero. *Nat. Rev. Chem.* **5**, 125–140 (2021).
20. Kozyryev, I. & Hutzler, N. R. Precision measurement of time-reversal symmetry violation with laser-cooled polyatomic molecules. *Phys. Rev. Lett.* **119**, 133002 (2017).
21. Kozyryev, I., Lasner, Z. & Doyle, J. M. Enhanced sensitivity to ultralight bosonic dark matter in the spectra of the linear radical SrOH. *Phys. Rev. A* **103**, 043313 (2021).
22. Anderegg, L. et al. An optical tweezer array of ultracold molecules. *Science* **365**, 1156–1158 (2019).
23. Zhang, J. T. et al. An optical tweezer array of ground-state polar molecules. *Quantum Sci. Technol.* **7**, 035006 (2022).
24. Isaev, T. A. & Berger, R. Polyatomic candidates for cooling of molecules with lasers from simple theoretical concepts. *Phys. Rev. Lett.* **116**, 063006 (2016).
25. Kozyryev, I., Baum, L., Matsuda, K. & Doyle, J. M. Proposal for laser cooling of complex polyatomic molecules. *ChemPhysChem* **17**, 3641–3648 (2016).
26. Augenbraun, B. L., Doyle, J. M., Zelevinsky, T. & Kozyryev, I. Molecular asymmetry and optical cycling: laser cooling asymmetric top molecules. *Phys. Rev. X* **10**, 031022 (2020).
27. Dickerson, C. E. et al. Franck–Condon tuning of optical cycling centers by organic functionalization. *Phys. Rev. Lett.* **126**, 123002 (2021).
28. Liu, Y. et al. Magnetic trapping of cold methyl radicals. *Phys Rev. Lett.* **118**, 093201 (2017).
29. Zeppenfeld, M. et al. Sisyphus cooling of electrically trapped polyatomic molecules. *Nature* **491**, 570–573 (2012).
30. Prehn, A., Ibrügger, M., Glöckner, R., Rempe, G. & Zeppenfeld, M. Optoelectrical cooling of polar molecules to submillikelvin temperatures. *Phys. Rev. Lett.* **116**, 063005 (2016).
31. Kozyryev, I. et al. Sisyphus laser cooling of a polyatomic molecule. *Phys. Rev. Lett.* **118**, 173201 (2017).
32. Baum, L. et al. 1D magneto-optical trap of polyatomic molecules. *Phys. Rev. Lett.* **124**, 133201 (2020).
33. Augenbraun, B. L. et al. Laser-cooled polyatomic molecules for improved electron electric dipole moment searches. *New J. Phys.* **22**, 022003 (2020).
34. Mitra, D. et al. Direct laser cooling of a symmetric top molecule. *Science* **369**, 1366–1369 (2020).
35. Cheuk, L. W. et al. λ-enhanced imaging of molecules in an optical trap. *Phys. Rev. Lett.* **121**, 083201 (2018).
36. Caldwell, L. et al. Deep laser cooling and efficient magnetic compression of molecules. *Phys. Rev. Lett.* **123**, 033202 (2019).
37. Langin, T. K., Jorapur, V., Zhu, Y., Wang, Q. & DeMille, D. Polarization enhanced deep optical dipole trapping of Λ-cooled polar molecules. *Phys. Rev. Lett.* **127**, 163201 (2021).
38. Wu, Y., Burau, J. J., Mehling, K., Ye, J. & Ding, S. High phase-space density of laser-cooled molecules in an optical lattice. *Phys. Rev. Lett.* **127**, 263201 (2021).
39. Anderegg, L. et al. Laser cooling of optically trapped molecules. *Nat. Phys.* **14**, 890–893 (2018).
40. Hutzler, N. R., Lu, H.-I. & Doyle, J. M. The buffer gas beam: an intense, cold, and slow source for atoms and molecules. *Chem. Rev.* **112**, 4803–4827 (2012).
41. Jadbabaie, A., Pilgram, N. H., Klos, J., Kotochigova, S. & Hutzler, N. R. Enhanced molecular yield from a cryogenic buffer gas beam source via excited state chemistry. *New J. Phys.* **22,** 022002 (2020).
42. Zhu, M., Oates, C. W. & Hall, J. L. Continuous high-flux monovelocity atomic beam based on a broadband laser-cooling technique. *Phys. Rev. Lett.* **67**, 46–49 (1991).
43. Barry, J. F., Shuman, E., Norrgard, E. & DeMille, D. Laser radiation pressure slowing of a molecular beam. *Phys. Rev. Lett.* **108**, 103002 (2012).
44. Yeo, M. et al. Rotational state microwave mixing for laser cooling of complex diatomic molecules. *Phys. Rev. Lett.* **114**, 223003 (2015).
45. Hemmerling, B. et al. Laser slowing of CaF molecules to near the capture velocity of a molecular mot. *J. Phys. B* **49**, 174001 (2016).
46. Truppe, S. et al. An intense, cold, velocity-controlled molecular beam by frequency-chirped laser slowing. *New J. Phys.* **19**, 022001 (2017).
47. Baum, L. et al. Establishing a nearly closed cycling transition in a polyatomic molecule. *Phys. Rev. A* **103**, 043111 (2021).
48. Zhang, C. et al. Accurate prediction and measurement of vibronic branching ratios for laser cooling linear polyatomic molecules. *J. Chem. Phys.* **155**, 091101 (2021).
49. Steinecker, M. H., McCarron, D. J., Zhu, Y. & DeMille, D. Improved radio-frequency magneto-optical trap of srf molecules. *ChemPhysChem* **17**, 3664–3669 (2016).
50. Berkeland, D. J. & Boshier, M. G. Destabilization of dark states and optical spectroscopy in Zeeman-degenerate atomic systems. *Phys. Rev. A* **65**, 033413 (2002).
51. Tarbutt, M. Magneto-optical trapping forces for atoms and molecules with complex level structures. *New J. Phys.* **17**, 015007 (2015).
52. Hummon, M. T. et al. 2D magneto-optical trapping of diatomic molecules. *Phys. Rev. Lett.* **110**, 143001 (2013).
53. Norrgard, E., McCarron, D., Steinecker, M., Tarbutt, M. & DeMille, D. Submillikelvin dipolar molecules in a radio-frequency magneto-optical trap. *Phys. Rev. Lett.* **116**, 063004 (2016).
54. Williams, H. et al. Characteristics of a magneto-optical trap of molecules. *New J. Phys.* **19**, 113035 (2017).
55. Devlin, J. A. & Tarbutt, M. R. Three-dimensional Doppler, polarization-gradient, and magneto-optical forces for atoms and molecules with dark states. *New J. Phys.* **18**, 123017 (2016).
56. Lim, J. et al. Laser cooled YbF molecules for measuring the electron's electric dipole moment. *Phys. Rev. Lett.* **120**, 123201 (2018).
57. Devlin, J. A. & Tarbutt, M. R. Laser cooling and magneto-optical trapping of molecules analyzed using optical Bloch equations and the Fokker–Planck–Kramers equation. *Phys. Rev. A* **98**, 063415 (2018).
58. Burchesky, S. et al. Rotational coherence times of polar molecules in optical tweezers. *Phys. Rev. Lett.* **127**, 123202 (2021).
59. Wall, M. L., Hazzard, K. R. A. & Rey, A. M. in *From Atomic to Mesoscale: The Role of Quantum Coherence in Systems of Various Complexities* (eds Malinovskaya, S. & Novikova, I.) Ch. 1 (World Scientific, 2015).
60. Dickerson, C. E. et al. Optical cycling functionalization of arenes. *J. Phys. Chem. Lett.* **12**, 3989–3995 (2021).

Methods

Photon cycling and rovibrational repumping

The main cycling transition used for CaOH laser cooling is the rotationally closed $\widetilde{A}(000)^2\Pi_{1/2}(J'=1/2, p'=+) \leftarrow \widetilde{X}(000)^2\Sigma^+(N''=1, p''=-)$ electronic transition at 626 nm. Vibrational levels are labelled as $(v_1 v_2^{\ell} v_3)$, where v_1, v_2 and v_3 are the vibrational quantum numbers for the symmetric stretch, the Ca–O–H bend and the antisymmetric stretch modes, respectively, and ℓ is the vibrational angular momentum. Vibrational branching ratios (VBRs) from the excited $\widetilde{A}(000)^2\Pi_{1/2}(J'=1/2, p'=+)$ state were determined using dispersed laser-induced fluorescence spectroscopy in ref. [48]. It was found that 10 vibrational levels (including the $\widetilde{X}(000)$ state) have branching ratios above about 5×10^{-5} and must be repumped to cycle about 10^4 photons before 1/e loss to vibrational dark states occurs. Owing to parity doubling in bending modes with angular momentum $\ell \neq 0$, both the $\widetilde{X}(01^10)$ and $\widetilde{X}(11^10)$ vibrational states require rotational repumping to address the $\widetilde{X}(N''=2, J''=3/2, p''=-)$ levels. Similarly, the $\widetilde{X}(02^20)$ and $\widetilde{X}(12^20)$ repumping lasers address the $\widetilde{A}(J'=1/2, p'=+) \leftarrow \widetilde{X}(N''=2, J''=3/2, p''=-)$rotational branch only[47]. All other repumping lasers drive rotational transitions from $\widetilde{X}(N''=1, J''=1/2, p''=-)$ and $\widetilde{X}(N''=1, J''=3/2, p''=-)$in the ground-state manifold.

The vibrational levels repumped during CaOH photon cycling and laser cooling are listed in Extended Data Table 1, along with the excited vibronic level and laser wavelength used for repumping. The excited states were chosen to maximize the strength (or similarly, the Franck–Condon overlap) of each repumping transition, which enables many of the transitions to be driven with low intensity relative to the 'main' 626-nm cycling laser (Fig. 1c). This is especially important given that frequency-broadened lasers are used to repump the MOT in the experiment.

To determine the mean number of photons scattered in our optical cycling scheme (Fig. 1c), we account for vibrational branching from both the $\widetilde{A}(000)^2\Pi_{1/2}$ state and the $\widetilde{B}(000)^2\Sigma^+$ state, which is driven by the $\widetilde{X}(100)$repumping laser and is therefore populated during approximately 1 out of every 18 photon scatters. The VBRs from $\widetilde{B}(000)^2\Sigma^+$ were reported in ref. [61]. The 'effective' branching ratios for the CaOH laser cooling cycle, which weight the branching ratios from $\widetilde{A}(000)$and $\widetilde{B}(000)$ according to the fraction of photons scattered through each state, are listed in Extended Data Table 1. The mean number of photons scattered before 1/e loss of molecular population after repumping N states is $\langle n_{\mathrm{scatt}}\rangle = (1-\sum_i^N \mathrm{VBR}_i)^{-1}$, where VBR_i is the VBR of the ith state addressed.

Because the $\widetilde{B}(000)$state is frequently populated and tends to decay at 555 nm to $\widetilde{X}(000)$, these 555-nm photons may be used for efficient background-free detection of the CaOH MOT.

CaOH production and buffer gas cooling

CaOH is produced in a copper buffer gas cell cooled to about 2 K by a circulating liquid ^{4}He pot. The cell length is 44.5 mm and the diameter is 43.2 mm. A calcium metal target is ablated with a roughly 20-mJ, 5-ns laser pulse at 532 nm. The gas-phase Ca reacts with H_2O vapour to form CaOH. The molecule production is enhanced by about tenfold by introducing approximately 800 mW of 657-nm light, addressing the $4s^2\ {}^1S_0 \rightarrow 4s4p^3P_1$ transition in atomic Ca, into the cell through a 4-mm aperture on the side of the cell, 6.35 mm from the front aperture[41,62]. The molecules are cooled by collisions with ^{4}He buffer gas, introduced to the cell at a flow rate of 7 standard cubic centimetres per minute. They exit the cell through a 7-mm-diameter aperture and pass through a 20-mm-long, 25.4-mm-diameter slowing cell with a 9-mm-diameter front aperture[40,63] before travelling to the MOT region 81 cm downstream. There is a 5-mm-diameter, 12.7-mm-thick aperture at the back of the cell through which the slowing lasers are aligned, minimizing heat loads on the cell owing to the slowing light.

Radiative laser slowing

A combination of frequency-doubled and frequency-summed fibre lasers, external cavity diode lasers and continuous-wave dye lasers are used to generate the light used for laser slowing, MOT and sub-Doppler cooling. Each laser beam passes through an acousto-optic modulator (AOM) or an optical shutter to allow rapid switching on and off. The lasers used for white-light radiative slowing are combined on dichroic beamsplitters and frequency broadened over about 300 MHz using high-modulation-index electro-optic modulators with a resonance frequency of about 4.6 MHz. After accounting for the 52-MHz spin-rotation splitting between the $\widetilde{X}(N''=1, J''=1/2, p''=-)$ and $\widetilde{X}(N''=1, J''=3/2, p''=-)$ ground states used for optical cycling, this corresponds to a velocity spread of 140 m s^{-1} addressable by the white-light broadened lasers. We find that optimal accumulation of slow molecules ($\lesssim$10 m s^{-1}) is obtained by detuning the main cycling laser to resonantly address only velocities above about 55 m s^{-1}, resulting in compression of the velocity distribution at lower velocities[46]. All repumping lasers are tuned to resonantly address molecules between approximately −10 m s^{-1} and 130 m s^{-1}, although power broadening enables significant slowing of molecules even outside this velocity range. Resonant addressing of small negative velocities is important because these same lasers are also used to provide repumping during MOT and sub-Doppler cooling.

Experimental details of the MOT

The MOT coils consist of two pairs of copper spirals bonded to aluminum nitride boards, similar to those in refs. [11,32]. Each spiral consists of 8 turns, with an inner diameter of about 23 mm and an outer diameter of about 45 mm. The two boards are spaced by 25.4 mm, and each board consists of two spirals separated by 1.6 mm. The axial magnetic field gradient produced by the coils is 4.7 G cm^{-1} A^{-1}. They are driven at 1.0 MHz with high-power radio-frequency amplifiers and can be switched off in about 50 μs. The coils are driven with a root-mean-square current of 1.8 A, corresponding to an axial field gradient of about 8.5 G cm^{-1}. Compensation coils are installed to reduce the ambient magnetic field to <0.1 G along all three principal axes. This is important for optimizing sub-Doppler cooling[10].

The MOT cooling laser light passes through a double-passed AOM, used to tune the frequency and power of the cooling beams. It then passes through a Pockels cell, driven with a square wave at 1.0 MHz to perform radio-frequency MOT polarization switching. An AOM is used to generate two frequency components, spaced by 52.1 MHz, that address the $\widetilde{X}(N''=1, J''=1/2, p''=-)$ and $\widetilde{X}(N''=1, J''=3/2, p''=-)$ground states for laser cooling and magneto-optical trapping. The two frequency components are combined in an evanescent fibre coupler, three outputs of which are used for the MOT beams.

Repumping of vibrational dark states in the MOT is done with the same repumping laser beams used for slowing, which resonantly address molecules near zero velocity after being white-light broadened (see above). Forces owing to the $\widetilde{B}^2\Sigma^+(000) \leftarrow \widetilde{X}^2\Sigma^+(100)$ repumping laser at 574 nm (see above) are non-negligible because approximately 5% of all photons scattered during the MOT are absorbed from this laser. This results in a significant force imbalance in the MOT if repumping of this state is done using only the slowing beam path. Therefore, resonant light addressing this repumping transition, with 52-MHz sidebands to excite both components of the photon cycling ground state, is combined with the vertical MOT beam and retroreflected, mitigating the force imbalance. Forces from all other repumping lasers, which contribute to only about 0.7% of photon scatters, are negligible.

MOT scattering rate and lifetime

To determine the scattering rate of the MOT, we measure the MOT lifetime using a photomultiplier tube, as described in the main text. By removing a number of repumping lasers in the MOT, the number of photon scatters, and therefore the lifetime, can be varied. This serves as a useful check on systematic errors in the scattering-rate measurement.

We take lifetime data with several combinations of repumping lasers. By repumping all states in Extended Data Table 1 up to $\widetilde{X}(12^00)$, we

achieve approximately 1,200 photon scatters before 1/e loss of molecules to vibrational dark states. From the fitted lifetime of 2.60(3) ms, we extract a scattering rate of $4.62(5) \times 10^5\ s^{-1}$ at a MOT power of 3 mW per beam. Adding repumping lasers up through $\tilde{X}(300)$enables approximately 4,600 photon scatters with a fitted lifetime of 10.1(2) ms, giving a scattering rate of $4.55(9) \times 10^5\ s^{-1}$. Finally, adding all repumping lasers enables approximately 12,000 photon scatters with a fitted lifetime of 25.7(6) ms, giving a scattering rate of $4.67(11) \times 10^5\ s^{-1}$. The excellent agreement between these values suggests that the MOT lifetime is dominated by loss to vibrational dark states, and helps to confirm the reliability of the photon number estimates. The scattering rate is extracted from a linear fit of the MOT lifetime versus number of photons scattered (including several other repumper combinations), giving a value of $4.6(1) \times 10^5\ s^{-1}$. The scattering rate during sub-Doppler cooling is extracted using a similar technique.

Number of trapped molecules

The number of molecules loaded into the MOT is estimated from the photon scattering rate and the magnitude of the collected fluorescence on the EMCCD. The collection efficiency of the imaging system, including transmission losses through the optics, is 0.15 ± 0.05%, determined from a combination of calibration measurements and estimates of the numerical aperture. Uncertainties in the quantum efficiency of the EMCCD are small in comparison. Numbers are determined from a 10-ms image of the MOT on the EMCCD, following a 5-ms loading ramp and a 10-ms hold time at 3 mW per MOT beam. The scattering rate at this intensity (also used during imaging) is $4.6(1) \times 10^5\ s^{-1}$, as described above. Owing to the background-free imaging scheme, only 1 out of every 18 photons is emitted at the detected wavelength of 555 nm. Combining these factors, the number of molecules detected on the EMCCD is $2(1) \times 10^4$. The error is dominated by the uncertainty in the collection efficiency of the imaging system.

Measurement of MOT oscillations and damping

The oscillation frequency and damping rate of the MOT are measured by waiting for the position of the CaOH molecular cloud to equilibrate after loading, then suddenly pushing the molecules in the direction of the slowing laser with a 1-ms-long pulse of slowing light. After a variable time, we image the cloud using a 1-ms exposure, which is short compared with the oscillation period, and extract the centre position using a 2D Gaussian fit. The observed maximum displacement increases with decreasing MOT intensity as the MOT forces weaken relative to the constant pushing force. Nonetheless, we find that the maximum displacement is $\lesssim$3 mm in all cases, implying that both the position, r, and velocity, $v = \dot{r}$, of the molecules is small enough that the MOT force may be Taylor expanded about $r = v = 0$ to yield[54]:

$$\ddot{r} + \beta\dot{r} + \omega^2 r = 0 \tag{1}$$

where β is the damping constant, ω is the oscillation frequency, and one or two dots denote a first or second-order derivative with respect to time. We fit the centre position of the CaOH molecular cloud, as a function of time, to the solution of equation (1) for an underdamped harmonic oscillator:

$$r(t) = r_0 + a e^{-\beta t/2} \sin\left(\sqrt{(\omega^2 - \beta^2/4)}\, t - \phi\right) \tag{2}$$

where r_0 is the equilibrium position, a is the amplitude and ϕ is a phase. The results of the fit, for various MOT intensities, are presented in the main text.

Temperature measurements

Temperatures are determined by waiting about 15 ms for the CaOH molecular cloud to thermalize after MOT loading, then turning off the MOT laser beams and magnetic field for a variable expansion time, τ_{TOF}. The molecules are then imaged by applying resonant light from the MOT beams for 1 ms, and its radial and axial widths, σ_ρ and σ_z, are fit from a 2D Gaussian model. The imaging time was chosen to be short compared with the TOF, and it was verified, by comparsion with images with even shorter exposures of 0.5 ms, that the imaged cloud size was unaffected by the imaging light.

After ballistic expansion during the TOF, the molecular cloud size along each axis is $\sigma^2 = \sigma_0^2 + k_B T \tau_{TOF}^2/m$, where σ_0 is the initial size and k_B is the Boltzmann constant. Therefore, the radial and axial temperatures were determined by linear fits of σ_ρ^2 and σ_z^2 versus τ_{TOF}^2 for each axis. The same procedure is used to extract temperatures after sub-Doppler cooling.

Data availability

The data that support the findings of this study are available from the corresponding author on reasonable request. Source data are provided with this paper.

61. Augenbraun, B. L. *Methods for Direct Laser Cooling of Polyatomic Molecules*. PhD thesis, Harvard University (2021).
62. Oberlander, M. D. & Parson, J. M. Laser excited fluorescence study of reactions of excited Ca and Sr with water and alcohols: product selectivity and energy disposal. *J. Chem. Phys.* **105**, 5806–5816 (1996).
63. Lu, H.-I., Rasmussen, J., Wright, M. J., Patterson, D. & Doyle, J. M. A cold and slow molecular beam. *Phys. Chem. Chem. Phys.* **13**, 18986–18990 (2011).

Acknowledgements We acknowledge B. L. Augenbraun and Y. Bao for discussions, and thank S. Kotochigova and J. Kłos for providing theoretical insight into the CaOH chemical enhancement. This work was supported by the AFOSR and the NSF. N.B.V. acknowledges support from the NDSEG fellowship, and L.A. acknowledges support from the HQI.

Author contributions N.B.V., C.H., L.A., P.R., A.W. and D.M. designed and assembled the apparatus, discussed experimental protocols and performed the experiment. N.B.V., C.H. and L.A. analysed the data. J.M.D. supervised all work and contributed to setting the direction of the experiment, as well as the design and development of the experimental apparatus, methods and analysis of data. All authors discussed the results and contributed to the manuscript.

Competing interests The authors declare no competing interests.

Additional information

Supplementary information The online version contains supplementary material available at https://doi.org/10.1038/s41586-022-04620-5.

Correspondence and requests for materials should be addressed to Nathaniel B. Vilas.

Peer review information *Nature* thanks the anonymous reviewers for their contribution to the peer review of this work. Peer reviewer reports are available

Extended Data Table 1 | Repumping transitions driven for CaOH photon cycling and laser cooling

Ground state	Excited state	Wavelength	"Effective" VBR
$\widetilde{X}(000)$	$\widetilde{A}(000)^2\Pi_{1/2}$	626.4 nm	0.9470(28)
$\widetilde{X}(100)$	$\widetilde{B}(000)^2\Sigma^+$	574.3 nm	0.0465(26)
$\widetilde{X}(02^00)$	$\widetilde{A}(100)^2\Pi_{1/2}$	629.0 nm	$2.58(16)\times10^{-3}$
$\widetilde{X}(200)$	$\widetilde{A}(100)^2\Pi_{1/2}$	650.4 nm	$1.71(16)\times10^{-3}$
$\widetilde{X}(01^10), N=1$	$\widetilde{B}(000)^2\Sigma^+$	566.0 nm	$8.2(4)\times10^{-4}$
$\widetilde{X}(02^20)$	$\widetilde{A}(100)^2\Pi_{1/2}$	630.0 nm	$6.4(1.1)\times10^{-4}$
$\widetilde{X}(01^10), N=2$	$\widetilde{A}(010)\kappa^2\Sigma^{(-)}$	622.9 nm	$3.6(2)\times10^{-4}$
$\widetilde{X}(12^00)$	$\widetilde{A}(020)\mu^2\Pi_{1/2}$	650.8 nm	$2.0(3)\times10^{-4}$
$\widetilde{X}(300)$	$\widetilde{B}(100)^2\Sigma^+$	594.3 nm	$6.5(8)\times10^{-5}$
$\widetilde{X}(11^10), N=1$	$\widetilde{A}(010)\mu^2\Sigma^{(+)}$	651.1 nm	$6.0(5)\times10^{-5}$
$\widetilde{X}(12^20)$	$\widetilde{A}(020)\kappa^2\Pi_{1/2}$	645.9 nm	$4.9(1.1)\times10^{-5}$
$\widetilde{X}(11^10), N=2$	$\widetilde{A}(010)\kappa^2\Sigma^{(-)}$	647.0 nm	$2.5(2)\times10^{-5}$

'Ground state' refers to the vibrational level of the $\widetilde{X}^2\Sigma^+$ electronic manifold, and 'excited state' gives the excited vibronic level to which the repumping transition is driven. The rotational level of each excited state is $\widetilde{A}(J'=1/2, p'=+)$. 'Effective' VBRs account for repumping through both the $\widetilde{A}$ and $\widetilde{B}$ states (see text).